energies

MDPI

Article

Impact of a Punching Process on the SyRM Iron Loss: SPICE Model as an Effective Tool for Iron Loss Modeling

Zbigniew Gmyrek

Institute of Mechatronics and Information Systems, Lodz University of Technology, 90 537 Lodz, Poland; zbigniew.gmyrek@p.lodz.pl; Tel.: +48-42631-2583

Abstract: Many technologies for cutting the magnetic laminations, from which electric motors cores are built, change material properties, among which are magnetizability and iron loss, thus affecting the motor parameters such as motor efficiency. This problem is particularly important for low-power motors, in which the dimensions of the magnetic circuit elements are relatively small. The correct estimation of the motor efficiency is important as early as at its design stage. This is possible when the correct material characteristics are used. This knowledge and analytical model enabling fast estimation of material properties (depending on the actual size) are necessary for engineers, who design electrical motors by analyzing many solution variants in a short time. The author proposes an analytical model of changing material properties, implemented in SPICE software. Its effectiveness was compared with measurement results while being a competitive solution in relation to other analytical models. The proposed SPICE model allowed evaluating material properties for lamination of any width. In the end, the knowledge concerning the material properties was used to calculate the iron loss in the stator of the SyRM motor, showing the need to use the material characteristics calculated for the specified width of the core piece.

Keywords: analytical methods; soft magnetic materials; synchronous reluctance motors; nondestructive testing

check for updates

Citation: Gmyrek, Z. Impact of a Punching Process on the SyRM Iron Loss: SPICE Model as an Effective Tool for Iron Loss Modeling. *Energies* **2021**, *14*, 7185. https://doi.org/10.3390/en14217185

Academic Editor: Issouf Fofana

Received: 3 September 2021
Accepted: 21 October 2021
Published: 2 November 2021

Publisher's Note: MDPI stays neutral with regard to jurisdictional claims in published maps and institutional affiliations.

Copyright: © 2021 by the author. Licensee MDPI, Basel, Switzerland. This article is an open access article distributed under the terms and conditions of the Creative Commons Attribution (CC BY) license (https://creativecommons.org/licenses/by/4.0/).

1. Introduction

For many years, designers of electric motors applied lamination characteristics obtained from catalogs or simple measurements performed using standard measuring systems, such as Epstein frame or single-sheet tester (single-strip tester) [1–3]. Sometimes ring cores were applied, although this is not a standard solution. Possible differences in the estimated motor's parameters were corrected by means of technological coefficients. At present, the problem of accurate determination of the electric motor efficiency is associated with the search for the most correct and precise approaches to determine all the loss components. As it is known, the iron losses are the most difficult to estimate, including both the iron loss, directly related to the main sinusoidal magnetic flux, and the additional losses, e.g., surface and pulsating losses, typically related at high-frequency flux pulsations. For laminations, this problem additionally complicates the fact of punching or laser cutting, the core assembly process (clamping, welding, gluing, etc.), and its positioning into the housing [4–6]. Available software tools and research results published by research groups, as well as the need for a quick analysis of many variants of calculations leading to an optimal structure of the electric motor, lead to the following conclusion: currently, desirable computational models should take into account the effect of the magnetic core's size and the used cutting technology on its material characteristics.

The need for a quick analysis of many calculation variants, solution optimizations, and coefficients to match the results of measurements and calculations inclines many researchers to use professional software, including blocks (collected from libraries) with vast configuration possibilities, both as to the area of application and functions. Expected features of such software include, for example, graphical interfaces for entering data,

many ready-made solvers, scripting language capabilities to write custom procedures, and a wide range of signal observations in the modeled object, including their analysis. For commonly used professional tools, we include, for example, MATLAB, often used in cooperation with Simulink, Mathematica, SPICE, Octave, Scilab, and other software. In this group, we can indicate the software such as MATLAB or Simulink intended for modeling physical phenomena and signals belonging to a broad research area [7–11] and SPICE dedicated to modeling and analyzing mainly electronic circuits. However, the literature provides many examples of much more expansive use of this tool, which exceeds far beyond electronics [12–17]. The need to have a mathematical model of a ferromagnetic material containing damaged material zones inspired the author to search for an application that allows for its implementation and quick analysis of the results (implemented using a script). A friendly application turned out to be ICAP/4, which belongs to the SPICE family.

For years, the exact determination of the properties of ferromagnetic materials used to build electric motor cores has been considered. It resulted from cognitive goals, and above all practical ones, related to the design of electric motors with increasing efficiency. This problem applies particularly to motors of relatively small dimensions, in which the most commonly used cutting technologies for shaping the magnetic circuit elements cause a noticeable deterioration of material properties. This deterioration translates into an increased magnetizing current, which, in turn, results in reduced motor efficiency, forcing designers to introduce new solutions and materials to meet the current requirements included in the IE3 and IE4 standardized efficiency classification. Therefore, extensive research was carried out to learn more about the reasons for changes in material properties and the effect of cutting technology [18–21]. In addition, intensive work on mathematical models describing these changes was carried out [22–24].

In this context, this paper proposes a mathematical model of property changes, applicable to punched laminations. This model is directly related to the results of simple noninvasive magnetic measurement, allowing direct determination of the basic parameters of the analytical model, which is a new solution compared with other analytical models described in the literature, where the measurement results are used only to determine fit coefficients. The proposed model was implemented in ICAP/4, which used the proprietary scripts to quickly and effectively analyze the results. The simulation results were compared with measurements, showing the usefulness and accuracy of the proposed analytical model.

The paper is organized as follows: Methodology and measurement results are described in Section 2; a mathematical description of the proposed analytical model and a brief reference to the existing analytical models are contained in Section 3; the implementation of the model in ICAP/4 software finds its detailed description in Section 4; Section 5 is dedicated to the model tuning, i.e., setting its parameters so as to achieve the highest possible simulation accuracy; subsequently, Section 6 contains simulation results and their comparison with measurement results; Section 7 shows the application of results obtained from the SPICE model, in the calculation of the reluctance motor's parameters; lastly, the whole work is summarized in the Conclusion Section.

2. Measurements in the Single-Strip Tester System

Soft magnetic materials are an essential construction element of electrical machines and transformers. It is known that their properties change depending on the production technology, lamination thickness, and working conditions (e.g., flux density level). For many years, producers determined material properties in the form of catalog curves, such as the specific iron loss or magnetization, in designing electric motors, transformers, and chokes. Such curves were determined for a specified frequency range, using standard measuring systems: Epstein frame or single-sheet tester. The size miniaturization of currently produced electric motors led to differences between the calculated parameters, e.g., motor efficiency, and measurements. There are many reasons for this situation, e.g., the need to take into account the core assembly process or the negative effects of cutting. In engineering practice, the usage of the single-sheet tester system can be problematic

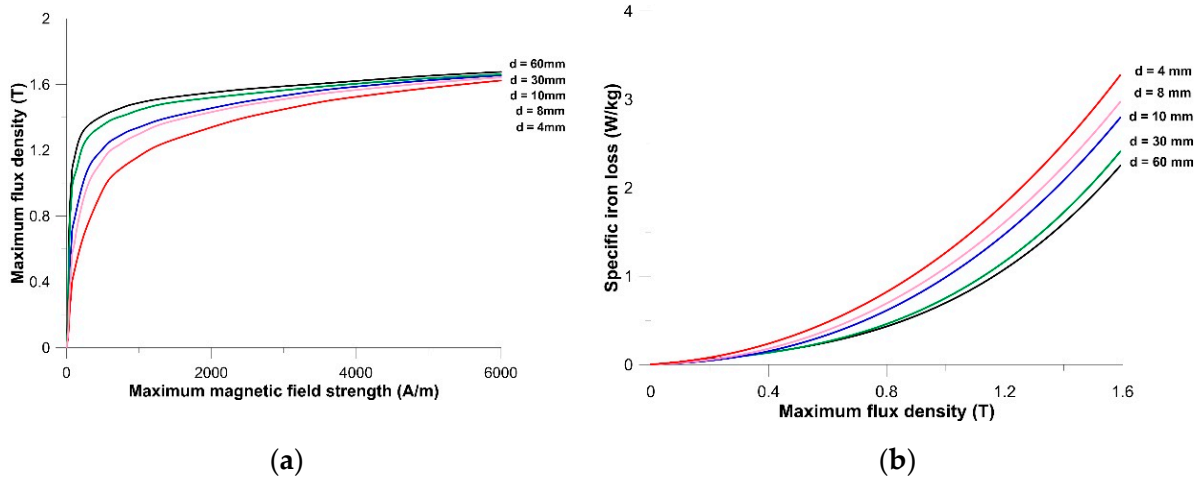
due to the relatively large dimension of the test sheet. Thus, instead of the mentioned system, the single-strip tester system was used, in which the ferromagnetic strips of much smaller sizes were used. Many years ago, the author of this paper proposed a measurement system with variable geometry (such as the aforementioned single-strip tester), allowing for the implementation of measurements with acceptable accuracy for strips with small sizes (see [3]). The mentioned system, described in detail in [3], allowed measuring the properties of M250-35A material. Strips of 300 mm long, thicknesses of 0.35 mm, and various widths, i.e., 60, 40, 30, 20, 10, 8, 6, and 4 mm, were tested. The tested material showed significant magnetic anisotropy; thus, the measurements were executed for the strips cut at an angle of 0 and 90 degrees, in relation to the rolling direction. To use the entire available measuring space (determined by the SST's yoke width), for strips with a width of less than 60 mm, more strips were used, e.g., two 30 mm width strips were tested simultaneously, reaching a total width of 60 mm. In the case of strips with a width for which the required 60 mm could not be achieved, this number was chosen to fit in the measuring yoke, e.g., for 8 mm wide strips, 7 strips were tested to yield a total width of 56 mm. During the measurements, the B vs. H curve and p vs. B were recorded (where B was the maximum induction averaged over strip cross section, H was the maximum magnetic field strength, and p was the specific iron loss of investigated material). In addition, the measurements for a strip of 60 × 300 mm, cut by the less-invasive water-jet technology, were executed. In this case, the measurement results were a reference base for the results obtained for punched strips. The small invasiveness of the water-jet technology confirmed by the measurement results of currently used various cutting techniques [25] authorized the author to accept the material of this strip as undamaged.

The tests were carried out at 50 Hz and 200 Hz, controlling the shape of the flux density waveform in strips (the induced voltage waveform in the measuring winding was recorded, and its shape was controlled). At the same time, the magnetizing current was recorded. It was the basis for calculating the maximum magnetic field strength in the strips and the specific iron loss of the investigated material, using the known relationship

$$p = \frac{N_{mag}}{N_{meas}} \frac{1}{V} \frac{1}{\sigma} \frac{1}{T} \int_0^T i_{mag}(t)\, u_{meas}(t)\, dt \tag{1}$$

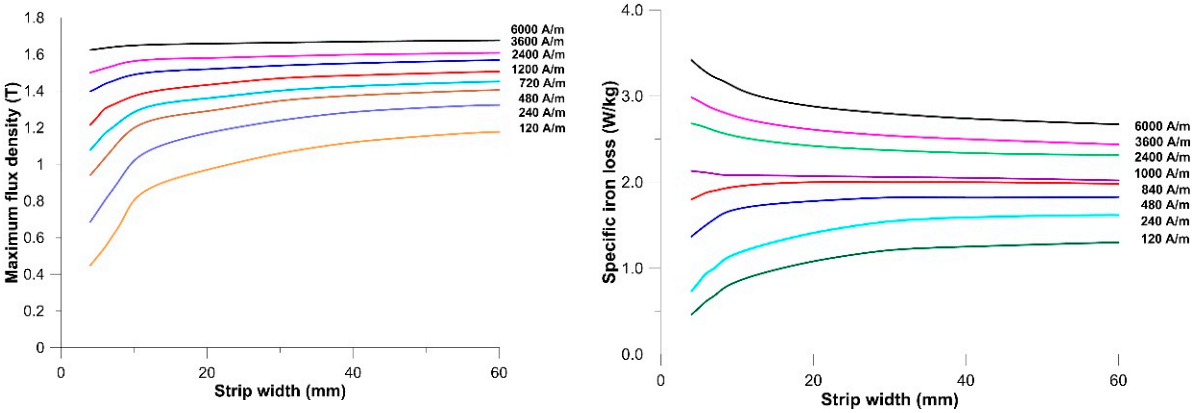
where p is the specific iron loss, N_{mag} is the turn number of magnetizing winding, N_{meas} is the turn number of measuring winding, V is the volume of the investigated strip (strips), σ is the material mass density, T is the waveform period, i_{mag} is the magnetizing current, and u_{meas} is the voltage induced in measuring winding.

Measurement results concerning strips of different widths, presented as the curves family B vs. H and p vs. B, are shown in Figure 1. It is much more interesting to present the same results for a specified value of magnetic field strength, shown as the curves family B vs. d and p vs. d, both for specified magnetic field strength (d is a strip width), in Figure 2. Such presentation of the measurement results is a part of the proposed new algorithm of the proceedings leading to direct reading of two model parameters (instead of searching them in the model optimization process). The magnetic flux density shown in Figures 1 and 2 represents the average flux density over the strip cross section.



(**a**) (**b**)

Figure 1. Measured curves for M250-35A material, cut at an angle of 0 degrees. The strip widths are shown in the image: (**a**) *B* vs. *H*; (**b**) *p* vs. *B* at 50 Hz.



(**a**) (**b**)

Figure 2. Measured curves for M250-35A material, cut at an angle of 0 degrees. Both curves family are presented for specified magnetic field strength: (**a**) *B* vs. *d*; (**b**) *p* vs. *d* at 50 Hz.

It can be seen in Figure 2 that for the strip width below 10 mm, both the specific iron loss and the maximum induction averaged over the strip cross section essentially change. These changes result from material property variation, partly damaged as a result of the punching process. The changes in the maximum flux density had the same character regardless of the magnetic field strength value: for a small strip width, the maximum induction reached values lower than for wider strips (for the same magnetic field strength). Additionally, attention should be paid to the different character of changes in specific material loss: for relatively large fields, the specific loss decreased with increasing the strip width; for relatively small strip width, the specific loss increased with the greater width. The observed result can be easily explained taking into account the course of the *B* vs. *d* curves shown in Figure 2a. We can see that for high magnetic field strengths, the average induction (in a strip's cross section) changes little along with the change in the strip's width. For medium and small magnetic field strengths, we can observe a dramatic decrease in the average induction—up to 40–50% in relation to induction for a strip of 60 mm width. In general, it is known that the destruction of the grain structure and the presence of internal stress caused by the cutting process lead to an increase in hysteresis and excess losses (both types of losses are joined with the movement of domain walls and therefore are susceptible to the aforementioned effects). Destruction and internal stress, and therefore the increase in losses, occur in the area near the edge. Thus, if the local

induction in the damaged area is comparable to induction in the undamaged area, the increase in material's specific loss will be visible for narrow strips (a relatively large share of the damaged area in a narrow strip)—this corresponds to the case of high magnetic field strength. If the local induction in the damaged area is significantly less than induction in the undamaged area, even after taking into account the increase in hysteresis and excess losses, the material's specific loss of a narrow strip will be less than those estimated for the wide strip, where the local induction is higher—this is the case for small magnetic fields. Measurement activity was completed by obtaining measurements of a 60 mm wide strip cut using the water-jet technology. Based on experience, the author concluded that this minimally invasive cutting method allows accepting the assumption that the results are equivalent to those for a "green" material, for example, obtained using a single-sheet tester system.

3. Mathematical Model Describing Changes in Properties of Materials in a Damaged Area

In the literature, there are many examples of the investigation results of researchers looking for effective analytical dependencies that enable determining material properties within the damaged area, where these properties change significantly. In order to avoid ambiguity of the induction amplitude distribution inside the ferromagnetic material, the models described in the literature or proposed in this paper refer to the case where the skin effect phenomenon is minimal and can be neglected. One example is an analytical model proposed by Sundaria et al., which is presented in [22] and developed in [26]. The form of the model was based on the authors' measurement results and can be expressed as [22]

$$\mu(H,x) = \mu_{nd}(H) \cdot \left(1 - e^{-ax} e^{-bH}\right) \tag{2}$$

where $\mu(H, x)$ is the magnetic permeability at H magnetic field strength and x distance from the cut edge, $\mu_{\mathrm{nd}}(H)$ is the magnetic permeability of undamaged material, dependent on H magnetic field strength only, a, b are fitting parameters.

$$p(B(H,x),x) = c \cdot \left(1 + e^{-dx}\right) \cdot B^2(H,x) \tag{3}$$

where $p(B(H,x),x)$ is the specific iron loss, $B(H,x)$ is the flux density at H magnetic field strength, x distance from the cut's edge, and c, d are fitting parameters.

Another group of researchers proposed to condition the magnetization curve by the $\eta(x)$ distribution function. The following expressions, therefore, describe the model [23]:

$$B(H,x) = \mu_0(\mu_{rnd}(H) - \Delta\mu_{cut}(H) \cdot \eta(x))\, H \tag{4}$$

where $\mu_{\mathrm{rnd}}(H)$ is the relative magnetic permeability for undamaged material at H magnetic field strength, $\Delta\mu_{\mathrm{cut}}(H)$ is the relative magnetic permeability drop, and $\eta(x)$ is the distribution function. The distribution function is defined as [23]

$$\eta(x) = 1 - \frac{x}{dd} - a\frac{x}{dd}\left(1 - \frac{x}{dd}\right) \tag{5}$$

where dd is the depth over which the material is degraded, and a is the fitting parameter.

Mentioned authors of the previous study introduced the following relationship describing iron loss in a partly damaged material [23]:

$$P(x) = a_2(x) \cdot B(H,x)^2 f + a_1\left(1 + a_3 B(H,x)^{a4}\right) \cdot B(H,x)^2 f^2 + a_5 B(H,x)^{1.5} f^{1.5} \tag{6}$$

where a_2 is the hysteresis coefficient being dependent on distance from the cut's edge, a_1, a_3, a_4, and a_5 are material coefficients, and f is the frequency.

Another group of researchers tried to find a proper relationship concerning change in iron loss, suggesting modified classical dependence [27]

$$P = a_1(x)\ B^{\alpha} f + a_2 B^2 f^2 + a_5 B^{1.5} f^{1.5} + a_2 a_3 B^{a4+2} f^2 \tag{7}$$

where $a_1(x) = a_{1ref} + mx$ is the hysteresis coefficient, $a_{1\mathrm{ref}}$ is a_1 axis crossing, and $x = l_{\mathrm{cut}}/m_{\mathrm{s}}$ is a cut-edge proportion, l_{cut} is the length of cut edges, m_{s} is a specimen mass. The last research group, with a short review of the analytical methods used, proposed to link a change in permeability and iron loss with degradation profile [24]

$$\gamma(x) = 1 - (1 - \gamma_s)\ e^{-\frac{x}{\delta s}} \tag{8}$$

where γ_{s} is the degradation factor (suggested as equals to 0), and δ_{s} is the degradation skin depth. Then, the B flux density profile can be directly linked to the degradation profile, and hysteresis loss can be expressed as [24]

$$P_h(x) = P_{hnd}\ /\ \gamma(x) \tag{9}$$

where P_{hnd} is the hysteresis loss for undamaged material, and $\gamma(x)$ is the degradation profile described by (8).

All analytical models presented above contain material coefficients or fitting parameters, which were determined based on measurement results. The analytical model proposed by the author of this paper uses B vs. d and p vs. d curves (established for a specified H magnetic field strength). The model contains a material coefficient, but instead of fitting parameters, it indicates how to measure other coefficients necessary to the correct model functioning. Similar to other models described above, the suggested analytical model adopts an exponential nature of magnetic permeability changes in the damaged material zone near the cut edge. Therefore, the accepted model of the flux density changes vs. the distance from the cut's edge has the following form:

$$B(x) = B_{green} - \left(B_{green} - B_0\right)\ e^{-\frac{x}{EW}} \tag{10}$$

where B_{green} is the flux density for undamaged material, B_0 is the flux density at distance $x = 0^+$, and EW is the effective width of the damaged zone.

The B_{green} value (for a specified magnetic field strength) can be found with a single-sheet tester. However, in practice, for calculation conducted with an engineering accuracy, it could be accepted as a flux density, obtained for a strip with a width of at least 150 mm or less, e.g., 60 mm cut with technology, resulting in negligible material damage (e.g., the water-jet cutting). The B_0 is a flux density obtained by extrapolating B vs. x curve to $x = 0$. Using an analogy to the mathematical description of exponential waveforms that are a time function (having a nonzero initial value), the author proposes to accept the EW parameter as a distance from the cut's edge, for which $B(x) = 0.632\ B_{\mathrm{green}} + 0.368\ B_0$. Then, the EW parameter can be treated as a time constant for an exponential curve, which is the curve of magnetic permeability change. This parameter should be found, e.g., by the least-squares method, using measurements and calculations with the proposed model.

Generally, the specific iron losses are defined by a three-component dependence. The dependence presented below contains coefficients, found for the test material, by utilizing the commonly used method of the iron loss component separation.

$$p(B) = c_h(B) * B^2 + c_e * B^2 + c_{ex}(B) * B^{1.5} \tag{11}$$

where $c_{\mathrm{h}}(B)$, c_{e}, and $c_{\mathrm{ex}}(B)$ are hysteresis, classical eddy current, and excess coefficients, respectively. For investigated undamaged magnetic material cut at 0 degrees, coefficients estimated for 50 Hz are following: the c_{e} material coefficient is equal to 0.09, the c_{ex}

coefficients are equal to 0.0725, where c_h depends on flux density, according to the following dependency (in the range of investigated flux density from 0.4 T to 1.6 T):

$$c_h = 0.753 + \frac{0.0498}{B^2} \quad (12)$$

The presence of a zone containing heterogeneously damaged material results in a material-specific loss increase. The reasons for this increase are known and include internal stresses and the associated with it material microhardness changes, destruction of the grain structure, and most importantly, an increase in the dislocation density in the crystalline structure. In all these components, "impact strength" is a function of a distance from a cut's edge. The above conclusions were formulated based on observations (measurements) made by the author or based on the results of research conducted by other authors [18–21].

As changes in magnetic permeability are similarly related to the reasons mentioned above, the author proposes to use an exponential dependence, referring to the hysteresis loss component (this component is joined, among other things, with the dislocation of the crystallographic structure and material internal stress). Then, the *p(B(x),f,x)* location-specific iron loss of a strip with damaged material zones can be presented in the form of the following equation:

$$p\Big(B(x), x, f\Big) = k_{inc}(x) * c_h(B(x), f) * B(x)^2 + c_e(f) * B(x)^2 + k_{inc}(x) * c_{ex}(f) * B(x)^{1.5} \quad (13)$$

where $B(x)$ is a local flux density, f is the frequency, $k_{\mathrm{inc}}(x)$ is the increase factor (the same for hysteresis and excess loss), defined as

$$k_{inc}(x) = 1 + a * e^{-\frac{x}{EW}} \quad (14)$$

where a is a fit coefficient—it should be found, e.g., using the least-squares method, comparing the measurement and simulation results, and EW is the effective width of the damaged zone (the same as in Equation (10)).

The p_{AV} average specific iron loss of a material for a strip of SW width is described with the following equation:

$$p_{AV}(B_{AV}) = \frac{1}{SW} \int_0^{SW} p(B(x), x)\, dx \quad (15)$$

where SW is a strip's width.

4. Implementation of the Analytical Model with SPICE Software

As described in the introduction, analytical models are effectively implemented in professional software, providing the use of ready-made solvers and postprocessors. In this study, the author used ICAP/4 (from the SPICE software family), generally intended for modeling and simulation of semiconductor elements and electronic circuits. Owing to the flexibility and adaptability of elements (parts) available in this software, such as controlled sources, it was possible to easily and quickly implement mathematical equations describing the change in the properties of a ferromagnetic material containing zones with various properties. The concept of a system implementing the analytical model described by Equations (10) and (13) is shown below.

The electric circuit presented in Figure 3 can be divided into several parts. The first part, containing a V2 source, R3 resistor, and C2 capacitor, implements Equation (10). The mathematical equation form, formally identical to the equation describing a transient in a serial RC circuit, powered by a constant voltage (after switching on), when the capacitor is precharged. The supply voltage of such a circuit is the equivalent of B_{green} (in Equation (10)), where B_0 corresponds to the voltage to which the capacitor is precharged.

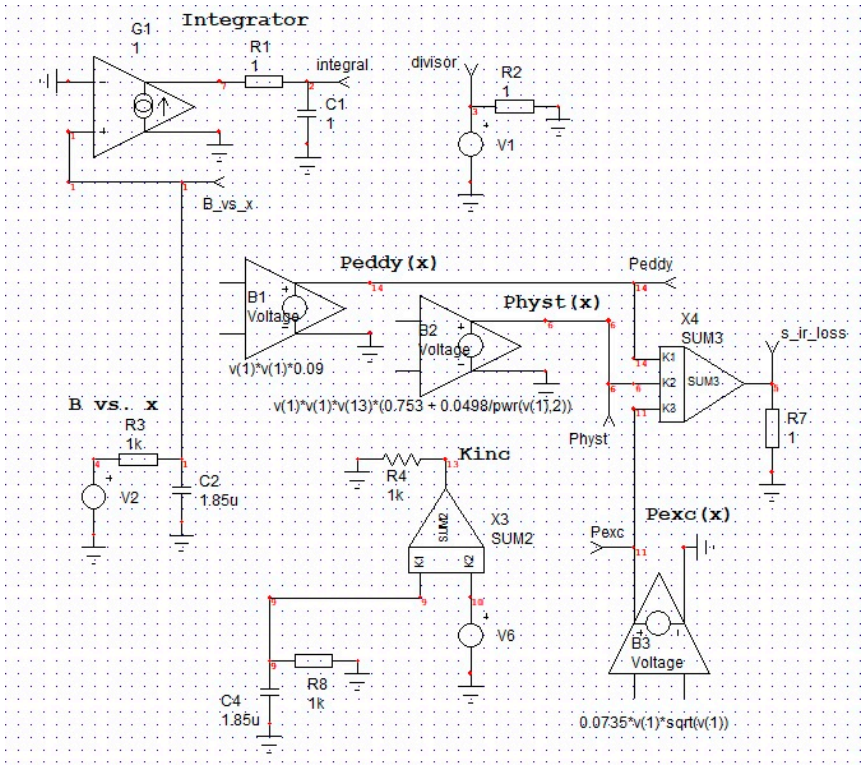


Figure 3. Electrical diagram of the circuit representing changes in the material properties of punched laminations.

The *EW* parameter existing in Equation (10) corresponds to a time-constant of this circuit (τ = RC), and the x variable (which indicates the distance from the cut's edge) is the equivalent of time. The output voltage of this circuit part (marked as "*B_vs_x*"), corresponds to the local induction, relating to the x distance from the cut's edge. Initial calculation data, i.e., the V2 source voltage (B_{green}) and the C2 capacitor precharge voltage (B_0), should be read from measurements (from B vs. x curve for a specific H), where the RC time-constant should be selected by best fit, using measurement and simulation data. Based on the measurements, using the curve shown in Figure 2a, B_{green} and B_0 were read. The B_{green} is a flux density, read from a strip cut with the water-jet technology, for a specified magnetic-field-strength value, and B_0 is a flux density obtained by extrapolating B vs. x curve to $x = 0$. The presented way constitutes the second part of the new proceedings' algorithm, enabling quick determination of two basic parameters of the analytical model used. Results are presented in Table 1.

The second part of the circuit presented in Figure 3, containing the G1 controlled source (transforming the voltage signal into the current one), the R1 resistor, and the C1 capacitor (forming the output signal marked as "integral"), performs integration of the "*B_vs_x*" signal. This circuit part marked as "Integrator", in cooperation with the V1 source and the R2 resistor (forming the output signal marked as "divisor"), is responsible for the preparation of the final integrated course. This course representing the induction averaged on x distance from the cut's edge is calculated in a postprocessor (using the "divisor" signal) and then used to compare with measurement results.

The "integral" signal is therefore described by the equation

$$u_C(t) = \frac{1}{C}\int i(t)\,dt \tag{16}$$

where $u_C(t)$ is the "integral" signal, and $i(t)$ is the "*B_vs_x*" signal.

Therefore, using signal names and changing t into x

$$\text{“integral”} = \frac{1}{C}\int \text{“}B_vs_x\text{”}dx \tag{17}$$

Table 1. Model data obtained as a result of direct measurements of the strips cut at an angle of 0 degrees.

Magnetic Field Strength	Magnetic Flux Density	
H (A/m)	B_{green} (T)	B_0 (T)
120	1.250	0.100
240	1.390	0.250
480	1.440	0.720
840	1.500	0.930
1080	1.523	1.010
2400	1.582	1.320
3600	1.616	1.440
6000	1.682	1.590

The third part of the circuit in Figure 3 includes programmable sources: B1, B2, and B3. Individual programmable sources enable determining the iron loss components—namely, eddy current, hysteresis, and excess losses. The sharing coefficients described by the defined formulas (12) and (13) were used in each source. The input data for these gates are the “B_vs_x” signal and the k_{inc} increase factor signal (this is an output signal of the X3 adding part, which implements Equation (14)). The X4 part sums the iron loss components, forming the “s_ir_loss” output signal specifying the local specific iron loss of the material. Then, this signal is averaged at an x distance (in the postprocessor). In this way, the specific iron loss of the x width strip is determined, enabling comparison with the measurement results.

5. Model Tuning

The first step was model tuning, i.e., determining a time-constant of a serial RC circuit (R3 and C2 parts). As mentioned earlier, using the best-fit method, the capacity of the C2 capacitor was matched (with the invariable R3 resistor value) to find a minimum error between the measured induction (averaged over the strip cross section) and the average induction obtained from the analytical model, taking all tested strips into consideration.

The relative error (specifying the model’s accuracy for indicated maximum field strength) was defined as

$$\varepsilon_B = \frac{1}{N}\sum_{i=1}^{N}\frac{\left(B_{i,\,meas} - B_{i,\,sim}\right)^2}{B_{i,\,meas}^2} \tag{18}$$

where N is the number of analyzed cases (number of strips having various widths), $B_{\text{i, meas}}$ is the measured flux density for a specified strip’s width, and $B_{\text{i, sim}}$ is the simulated flux density for a specified strip’s width.

The search result of the optimal time-constant value (for all measurements of various magnetic field strengths and strip widths) was 1.85 ms, which corresponded to the EW effective width of the damaged material zone. This time constant corresponded to the following values: the R3 resistor of 1 Ω and the C2 capacitor of 1.85 μF. It should be emphasized that tuning results were excellent, i.e., for the magnetic field strength greater than 1000 A/m, the relative error was close to zero; for a magnetic field strength in the range of 240–1000 A/m, the error was less than 0.05%, and for the magnetic field strength of 120 A/m, it amounted to 2.47%—detailed error results are shown in Table 2. The average

value of this error, amounting to 0.57%, was a minimum value when searching for the optimal value of the *EW* effective width. A slightly worse accuracy of the model, for small magnetic field strength, results from the nature of the phenomenon, i.e., smaller mobility of the Bloch walls, which causes the abandonment of exponential curve shape, representing the change in induction as the function of the distance from the cut's edge—the model should be extended to take this phenomenon into account. Due to the practical range of inductions used in electrical devices and motors, further expansion of the model in low inductions was not considered in this paper. After determining the effective width of the damaged material's zone (equivalent to the time constant), using the one previously calculated for undamaged material with the c_h, $c_{E,}$ and c_{EX} coefficients (Equation (13)), the specific iron loss of the material tested was calculated. The calculations demonstrated that the specific loss of the material for a wide strip obtained from the model is very close to this one, originating from the measurement. For a narrow strip, the specific loss calculated is less than the measured. The reason for this is the local increase in the specific loss of the material belonging to the damaged zone. The growth coefficient (Equation (14)) was sought to minimize the error of the average specific loss calculation (averaged over strip cross section). This error, calculated according to Equation (19), is shown in Table 2.

$$\varepsilon_p = \frac{1}{N}\sum_{i=1}^{N}\frac{\left(p_{i,\,meas} - p_{i,\,sim}\right)^2}{p_{i,\,meas}^2} \tag{19}$$

where N is the number of analyzed cases, $p_{\mathrm{i,meas}}$ is the measured specific loss for defined strip width, and $p_{\mathrm{i,sim}}$ is the simulated specific loss for defined strip width.

Table 2. The relative errors obtained during model tuning (at 50 Hz, strips cut at an angle of 0 degrees).

Magnetic Field Strength	Flux Density Error	Specific Iron Loss Error
H (A/m)	ε_B (%)	ε_P (%)
120	2.47	0.63
240	0.03	0.06
480	0.05	0.05
840	0.02	0.03
1080	~0	0.01
2400	~0	~0
3600	~0	~0
6000	~0	~0

The maximum value of the k_{inc} growth coefficient of the hysteresis loss, equal to 1.80, allowed to minimize the abovementioned error for all strips cut at an angle of 0 degrees and all maximum field strengths analyzed—then, this average error equals 0.1%.

In addition, a similar model tuning analysis was carried out for the measurement results obtained at a frequency of 200 Hz, achieving satisfactory accuracy.

6. Calculation Results

Employing the analytical model described and its coefficients found in the model tuning process, the local induction profiles vs. distance from the cut's edge were calculated for various magnetic field strengths, changing within the range of 120–6000 A/m. Then, the material-specific loss profiles were found in the same way. The proposed model ensured the implementation of calculations for half the width of the strip, accepting symmetrical local distributions of induction and specific iron loss, which were only dependent on a distance from the cut's edge. Example distributions, determined for the model representing

strips cut at 0 degrees, are shown in Figures 4–6. The magnetic permeability change in a part of the material, which results from the cutting process carried out, is the cause of changes in the magnetic induction amplitude and the distance from the cutting edge of the strip. In Figure 4, we can see that even for a 60 mm wide strip, an omission of the damaged material zone is not recommended. For the mentioned strip width, the average flux density is 2% lower than local flux density, while for a 6 mm wide strip, this difference reaches 10%. In a real magnetic circuit, depending on the induction level, this can cause negligible or even a change of several percentages in magnetic field strength value (magnetizing current). Otherwise, in the case of specific iron loss profiles, depending on the applied magnetic field strength, the average specific loss may be greater or smaller than the local one. There is a specific magnetic field strength for each material, above which the average specific iron loss is greater than the local one. For smaller field strength, the average specific iron loss is smaller than the local one. This effect does not occur in undamaged material.

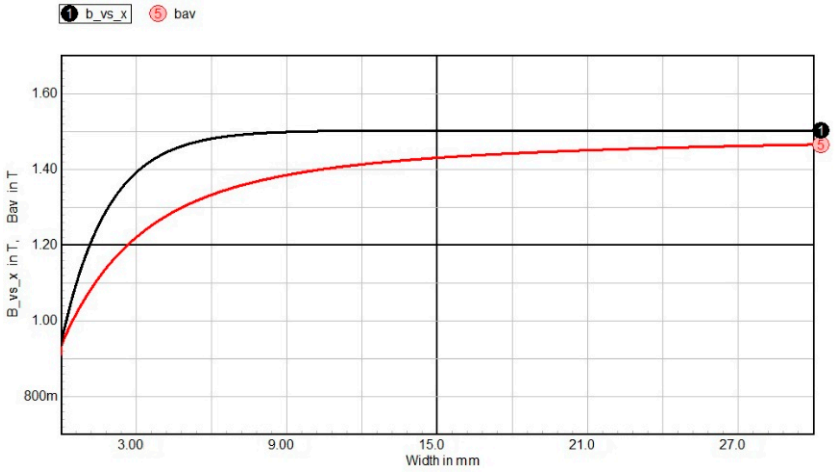


Figure 4. The amplitude profiles of local (black) and average flux density (red) (over an actual strip width), obtained from the analytical model (H_{max} = 840 A/m). The strips cut at an angle of 0 degrees. An image from the ICAP/4 postprocessor.

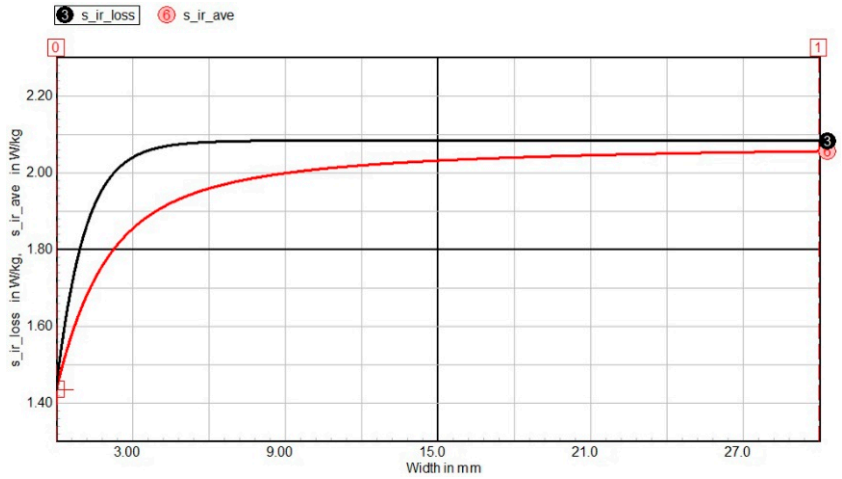


Figure 5. The profiles of local (black) and average specific iron loss (red) (over an actual strip width), obtained from the analytical model (H_{max} = 840 A/m, 50 Hz). The strips cut at an angle of 0 degrees. An image from the ICAP/4 postprocessor.

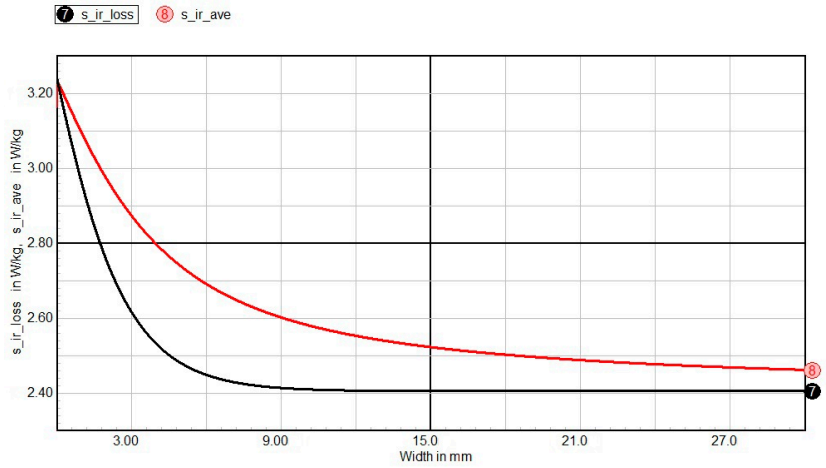


Figure 6. The profiles of local (black) and average specific iron loss (red) (over an actual strip width), obtained from the analytical model ($H_{\max}$ = 3600 A/m, 50 Hz). The strips cut at an angle of 0 degrees. An image from the ICAP/4 postprocessor.

Figures 5 and 6 show two cases. For the tested material, the boundary value of the magnetic field strength, for which despite the presence of the damaged material zone, the specific iron loss remains virtually constant (from x~0 mm to 30 mm), is 1000 A/m. This value depends on the strip thickness and the chemical composition of the material.

Figure 7 compares the simulation results and measurement of a magnetic induction (averaged over strip cross section), whereas a specific iron loss comparison is presented in Figure 8. As we can see, the chosen method of selecting model parameters, based on direct use of measurement results as well as adjustment of the model parameters, is effective in a wide range of changes in magnetic field strength. For this reason, it can be effectively used during design, for example, electrical motors or other devices containing magnetic circuits.

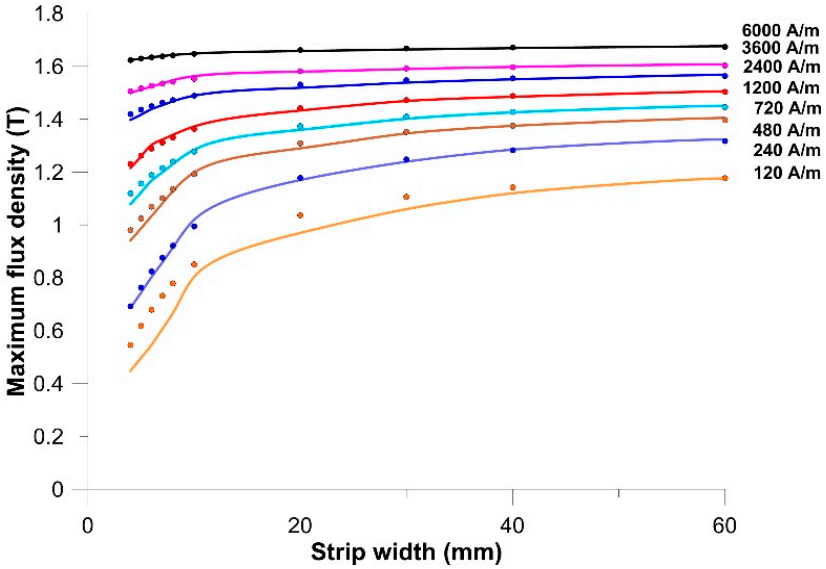


Figure 7. Comparison of the average flux density amplitude. The measurement (lines) and simulation (points) results. The strips cut at an angle of 0 degrees. Magnetic field strength changed in the range from 120 A/m to 6000 A/m.

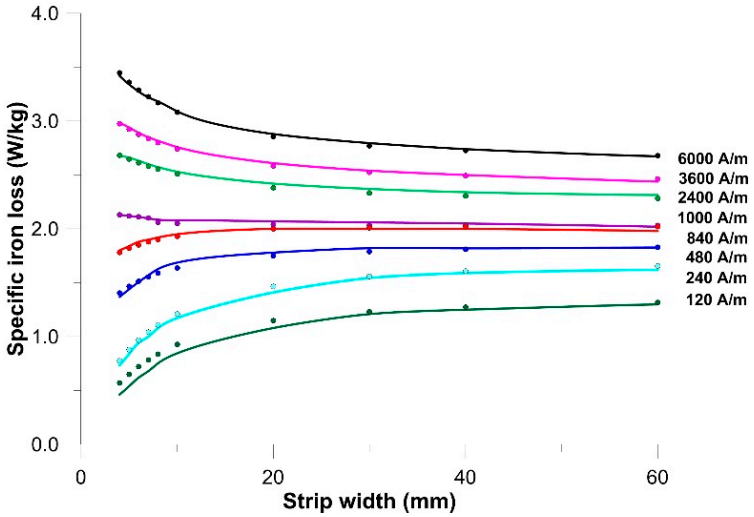


Figure 8. Comparison of the average specific iron loss, at 50 Hz. The measurement (lines) and simulation (points) results. The strips cut at an angle of 0 degrees. Magnetic field strength changed in the range from 120 A/m to 6000 A/m.

Comparison of calculation and measurement results obtained at the magnetic field strength of 120 A/m, presented in Figure 7, shows slightly worse effectiveness of the model used. According to the author's knowledge, this is due to the increasing importance of internal stresses when reducing the magnetic field strength. Similarly, the increase in dislocation density, resulting from partial destruction of the grain structure, becomes more and more visible. Both of these factors lead to a reduction in magnetic permeability. This fact should be considered in the next stage of the work, creating a more extensive analytical model.

7. Application of Results Obtained from the SPICE Model to SyRM Calculations

A built model describing changes in the material properties, implemented in the SPICE environment, was effectively used during calculations executed for a three-phase, four-pole, 120W synchronous reluctance motor (SyRM). The currently analyzed motor belongs to a group of mass-produced, low-power, line-start, synchronous reluctance motors (this motor contains the rotor cage enabling asynchronous start-up). Both during simulation (currently and previously applied) and in previously implemented measurements described in [28,29], the motor was devoid of a cage. In the original version, this motor was powered by the 400 V/50 Hz mains (Y winding configuration), and its core was built of M600-50A laminations. Its main dimensions are as follows: the outer stator diameter–106 mm, the core length–35 mm, frame size 71 mm. Currently, it is intended to adopt this construction to work at a higher frequency, first, by renewing the core's material, which is proposed to be M250-35A material. In this context, the presented SPICE model, enabling rapid determination of test material characteristics, was effectively used. It should be emphasized that this type of motor has already been examined in other aspects, in cooperation with a wider group of researchers [28–30].

The decisive factor affecting the need to use the SPICE model (or another model allowing a quick determination of the material characteristics) is the relatively small size of the motor core's elements. In the investigated motor, the width of the stator tooth was only 3.2 mm, and the width of the stator yoke was 7.35 mm. Corresponding rotor dimensions were 3.4 mm and 13 mm. As shown in completed measurements, it is necessary to consider the current width of the core fragment in its material characteristics used during calculations.

An important aspect of the analysis is acceptance of the change range that can be implemented. In the tested motor, the stator winding was the basic element generating power loss. According to the tests carried out for rated conditions (50 Hz), the Joule losses

approximately amount to 70% of the motor's rated power, causing relatively low motor efficiency—62%. At the same time, the sum of the mechanical loss and the iron core loss, constitute 15% of the mentioned Joule loss. Thus, any changes in the motor structure should not significantly change the Joule loss in the winding. In the new version of the motor, a preliminary solution changes the winding configuration to Delta connection, and the motor power supply changes to 600 V/200 Hz voltage. In the next steps, a small adjustment of the number of windings may be necessary.

The proposed M250-35A material is characterized by a relatively large magnetic anisotropy. The effective usage of this material in the performed calculations needed the execution of the measurements at 200 Hz, for strips cut at an angle of 0 and 90 degrees (with respect to the rolling direction). Then, the *B*0/90_vs. *d* curves family were determined (*d* is the width of the strip), using average measurements carried out on both types of strips (0 and 90 degrees)—see Figure 9. The indicated curves were determined for expected magnetic field values; an example of field strengths is shown in Figure 9. Then, the *B*0/90_vs. *H* and *p*0/90_vs. *B* curves were determined for the stator core's portions comprising a width of 3.2 mm and 7.4 mm, and rotor core's portions comprising a width of 3.4 mm and 13 mm; see Figure 10.

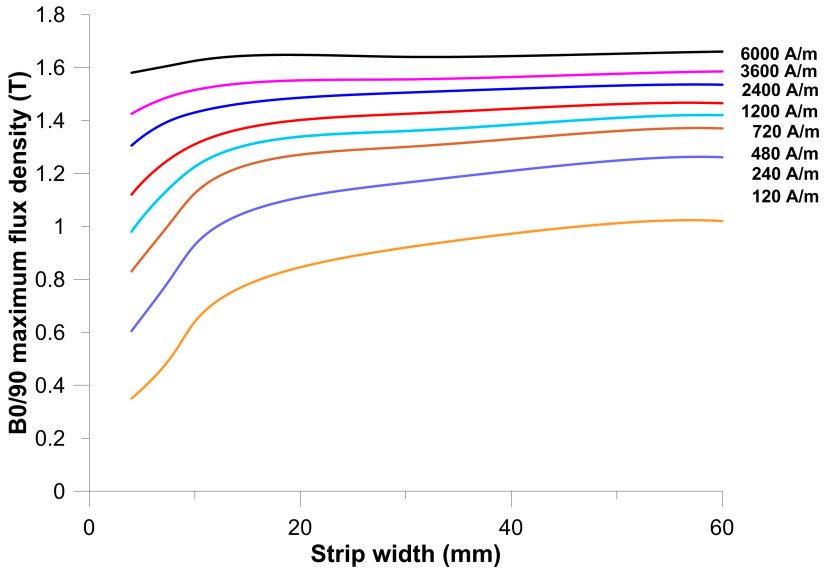
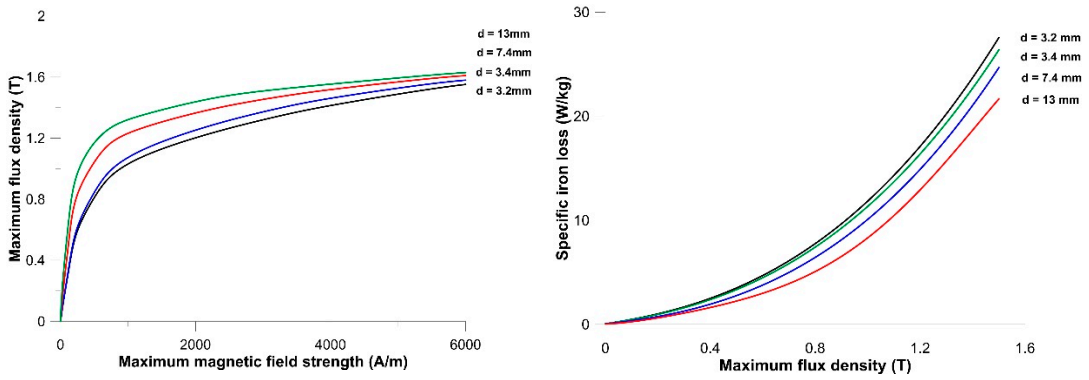


Figure 9. Calculated *B*0/90 maximum flux density curves for M250-35A material. The specified magnetic field strengths are shown in the image.



(**a**) (**b**)

Figure 10. Calculated curves for M250-35A material. The core's portions widths are shown in the image: (**a**) *B*0/90 vs. *H*; (**b**) *p*0/90 vs. *B* at 200 Hz.

The material characteristics obtained from the SPICE model (shown in Figure 10), were used in the FEM 2D model, created with the help of the professional Opera2D software. The author recognized that during the currently conducted research, the two-dimensional FEM model was sufficient to consider the motor geometry and estimation of the stator core's loss. The fundamental problem that appeared during the FEM model creation was a way to include the degree of the material damage as a function of the distance from the cut's edge. Four approaches were possible: the first in which the size and the equivalent properties of a homogeneously damaged area were defined; the second, where the division of the damaged area to sub-areas was used. These homogeneously damaged sub-areas were marked with known equivalent properties; the third used a software application that allowed the definition of local properties of the individual elements of the model mesh; the fourth approach allowed the use of a homogeneous material in a particular area, whose properties depend on its size. The second and third approaches require knowledge of local material properties. The fourth approach provides the possibility to use the average material properties, valid for specified size—compare the courses in Figures 4–6. Exploiting the previously described SPICE model, operating on the basis of a limited number of measurements carried out in the SST system, the material's characteristics were easily determined for elements having specified widths; see Figure 10. Therefore, the author used the fourth approach to take into account changes in the properties of the material, realizing that local magnetic induction and core loss can deviate from those that would be obtained using the model that assigned local material properties to the individual elements of the model mesh. The built FEM model enabled the rotor movement and its free positioning relative to the magnetic field, relevant to the adopted load torque. In order to facilitate meshing during the rotor movement, the air gap region was subdivided into three concentric layers. The numerical problems were solved by forcing a sinusoidal voltage supply—an example flux density distribution is visible in Figure 11. At the same time, the field and the coupled circuit models were solved. The stator core loss was calculated by (20), specifying the mass for each mesh element and assigning a specific loss curve (indicated for the element belonging to a specific area), determined based on the SPICE model. This was carried out in the postprocessor by finding the maximum value of the flux density in each mesh element.

$$P_{core} = \sum_{i=1}^{n} p(B_i, k)\, m_i \tag{20}$$

where P_{core} is the stator core loss, n is the number of the core pieces for which the stator core was divided, $p(B_i, k)$ is the specific iron loss, depending on B_{i} actual flux density and k core's region (tooth or yoke), and m_i is the mass of the actual core element.

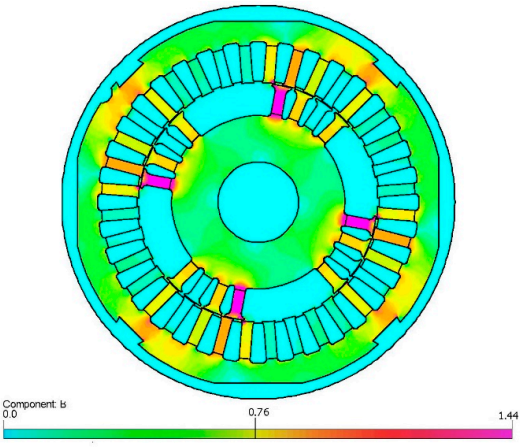


Figure 11. Calculated distribution of the magnetic induction (200 Hz, load torque equals 0.5 T_{n}).

As a result of the calculations carried out, the iron loss in the stator core (caused by the fundamental harmonic of the magnetic flux) was estimated and is presented in Table 3. In addition, the iron loss in the motor core made of M600-50A material (calculated at 50 Hz, obtained in previous investigations), were compared with those in the motor core made of M250-35A material (calculation carried out at 200 Hz, the number of coils was reduced by about 10%, and the winding Joule loss increased by 5%). The total stator core loss calculated in the previous investigation (at 50 Hz, M600-50A material) showed very good convergence with measurement results [31], reinforcing the author's conviction about the correctness of the model and the method used. In the literature, a description of other studies implemented in a similar way can be found. First, measurements of the specific loss and material-magnetizing curves for rectangular specimens with different widths are performed. These results are used during FEM calculation of the iron loss, executed for the core having a much more complicated shape. Then, the obtained results are compared with the measurement results. In practice, a two-subregion model is used, i.e., containing a damaged fragment with homogeneous material properties and the remaining part that is undamaged. As these examples show, even such a simplified approach guarantees the achievement of acceptable accuracy of the results obtained [22,27,32,33]. The herein presented paper uses a different approach, using a homogeneous material with its characteristics depending on the current width of selected subregions. The area of application of such an approach must be checked each time (comparing with the results obtained, e.g., from the two-subregion model).

Table 3. The iron loss in the stator core estimated at 50 and 200 Hz.

	M600-50A, 50 Hz	**M250-35A, 200 Hz**
Mass of the stator core's teeth (kg)	0.348	0.348
Mass of the stator core's yoke (kg)	0.610	0.610
Iron loss in the teeth (W)–undamaged material	1.60	4.02
Iron loss in the yoke (W)–undamaged material	2.08	3.78
Total iron loss (W)–undamaged material	3.68	7.80
Iron loss in the teeth (W)–damaged material	2.81	6.61
Iron loss in the yoke (W)–damaged material	3.36	6.10
Total iron loss (W)–damaged material	6.17	12.71

8. Discussion

The necessity to have an effective analytical model that ensures engineering calculation accuracy, combined with an easy way of parameters determination (based on a limited number of measurements), results from the needs of design offices, for example, for designing energy-saving electric motors. Selecting the size of structural elements, such as magnetic circuits, is one of the fundamental actions in the construction process. The change in the element's size generates the need to change material characteristics, such as magnetization and specific iron loss curves. In this case, relying on the material characteristics obtained on the measuring path for specimens with a given width (other than needed) leads to erroneous results, such as unacceptable errors in the range of several to a dozen percent in the case of energy-saving motors.

A reasonably important model parameter is the hysteresis loss's increase coefficient, resulting from the grain size or the grain destruction of the material parts [34]. In the

literature, we find the results of measuring the iron loss components, concerning the material with similar properties, showing that the increase in the hysteresis loss (averaged over the strip cross section) depends on the strip's width. For example, for an average magnetic induction of 1 T and strip width of 5 mm, the increase in hysteresis loss is 1.51 [35]. As the reference value, the authors used a hysteresis loss measured for a punched strip of 60 mm width. The research currently carried out shows that they made an error of a few percentages in estimating the increase coefficient. In the proposed model, the increase in hysteresis loss calculated according to Equation (14) is 1.43. In another publication [19], we found test results concerning changes in dislocation density in a part of the material close to the cut's edge. A hysteresis loss, among others, depended on the dislocation density. According to [19], hysteresis loss was enlarged 1.74 times. In the analytical model used, the maximum value of the hysteresis loss increase is 1.8 and therefore corresponds very well to the value mentioned above.

After the model's tuning, both the magnetic flux density and the material's specific iron loss, calculated and measured for the indicated strip widths and various magnetic field strengths, show very good convergence. This convergence is represented by the errors shown in Table 2. The maximum error reaches approximately 2.5% and definitely decreases with the increase in the magnetic field strength.

The presented results of iron loss estimation of the tested motor indicate an urgent need to update motor models (both analytical and FEM). The update applies to material characteristics used during calculations, which should be the function of the dimension (width) of the magnetic core fragment. An effective path that allows the use of such characteristics in relation to FEM models is still open and requires further testing. It should be emphasized that consideration of the usage of the ferromagnetic element size in material characteristics makes sense only when this size is comparable to the dimension of the damaged material zone (depending on the cutting technology used). In the presented work herein, the iron loss originating from the fundamental harmonic of the magnetic flux was analyzed, both for the adoption of the characteristics of undamaged and damaged material. In addition, a more intensive analysis of the impact of cutting on additional losses resulting from the magnetic flux pulsation is expected in subsequent works.

9. Conclusions

This paper presented an analytical model, implemented in ICAP/4, that described changes in the magnetic permeability and specific iron loss of the material subjected to the punching process. The proposed model was based on exponential dependence of the change in the material properties vs. a distance (this is a widely accepted dependence), combined with a new proceedings procedure when determining the basic model parameters. This procedure used measurement data directly, under certain conditions, which is not described in the literature. Other parameters, with less validity, were determined in a widely described traditional manner (model matching method). The results obtained regarding the effective width of the damaged material area are in line with the results reported by other researchers. The proposed analytical model is useful for engineers working in design firms and research centers requiring engineering accuracy. Owing to the speed of operation, consequent to the model's implementation in the ICAP/4, the model enables swift generation and analysis of the material characteristics of a ferromagnetic strip with a given width subjected to a punching process. The used SPICE model allowed the quick generation of material characteristics used in the FEM model. The obtained results show an increase of a few dozen percentages in the core loss while pointing to the need to take into account the size of ferromagnetic elements in its material characteristics used for calculations.

Funding: This research was funded by National Science Centre (NCN) Poland as part of the "Opus –18", Grant Number 2019/35/B/ST8/00764 "The manufacturing technology impact analysis of small-power high-speed electric motors to refine their analytical models.

Institutional Review Board Statement: Not applicable.

Informed Consent Statement: Not applicable.

Data Availability Statement: Not applicable.

Conflicts of Interest: The author declares no conflict of interest.

References

1. International Electrotechnical Commission. *Methods of Measurement of the Magnetic Properties of Magnetic Sheet and Strip by Means of a Single Sheet Tester, Standard IEC 60404-3*; International Electrotechnical Commission: Geneva, Switzerland, 2010.
2. International Electrotechnical Commission. *Methods of Measurement of the Magnetic Properties of Electrical Steel Strip and Sheet by Means of an Epstein Frame, Standard IEC 60404-2*; International Electrotechnical Commission: Geneva, Switzerland, 2008.
3. Gmyrek, Z. Single Sheet Tester with variable dimensions. *IEEE Trans. Instrum. Meas.* **2016**, *65*, 1661–1668. [CrossRef]
4. Fujisaki, K.; Hirayama, R.; Kawachi, T.; Satou, S.; Kaidou, C.; Yabumoto, M.; Kubota, T. Motor core iron loss analysis evaluating shrink fitting and stamping by finite-element method. *IEEE Trans. Magn.* **2007**, *43*, 1950–1954. [CrossRef]
5. Oka, M.; Kawano, M.; Shimada, K.; Kai, T.; Enokizono, M. Evaluation of the magnetic properties of the rotating machines for the building factor clarification. *Electr. Rev.* **2011**, *87*, 43–46.
6. Gmyrek, Z.; Lefik, M. Influence of Geometry and Assembly Processes on the Building Factor of the Stator Core of the Synchronous Reluctance Motor. *IEEE Trans. Ind. Electron.* **2017**, *64*, 2443–2450. [CrossRef]
7. Mandache, L.; Topan, D. Managing eddy current losses and ferromagnetic material nonlinearities in distorting regimes. In Proceedings of the IEMDC, Miami, FL, USA, 3–6 May 2009; pp. 1449–1454. [CrossRef]
8. Mandache, L.; Topan, D.; Iordache, M.; Sirbu, I. SPICE model for effective and accurate time domain simulation of power transformers. In Proceedings of the Joint INDS'11 & ISTET'11, Klagenfurt, Austria, 25–27 July 2011; pp. 1–6. [CrossRef]
9. Kumar, R.; Saxena, R. Simulation and analysis of switched reluctance motor drives for electric vehicle applications using MATLAB. In Proceedings of the ICEECCOT, Mysuru, India, 13–14 December 2020; Volume 19688723. [CrossRef]
10. Preethishiri, R.S.; Roseline, J.A. Switched reluctance motor (SRM) development by using Matlab-Simulink. In Proceedings of the ICPEDC, Chennai, India, 21–23 August 2019; Volume 19455729. [CrossRef]
11. Saeed, S.; Garcia, J.; Georgious, R. Modeling of variable magnetic elements including hysteresis and eddy current losses. In Proceedings of the APEC Conference, San Antonio, TX, USA, 4–8 March 2018; Volume 17719483. [CrossRef]
12. Abramovitz, A.; Ben-Yaakov, S. RGSE-Based SPICE model of ferrite core losses. *IEEE Trans. Power Electr.* **2018**, *33*, 2825–2831. [CrossRef]
13. Detka, K.; Gorecki, K.; Zarebski, J. Modeling single inductor DC–DC converters with thermal phenomena in the inductor taken into account. *IEEE Trans. Power Electr.* **2017**, *32*, 7025–7033. [CrossRef]
14. Gupta, O.; Sheel, S. Control of induction motor drive with PSpice-MATLAB interfacing. In Proceedings of the PEDES, Bengaluru, India, 16–19 December 2012; Volume 13400162. [CrossRef]
15. Fujiwara, T.; Tahara, R. Eddy current modeling of silicon steel for use on SPICE. *IEEE Trans. Magn.* **1995**, *31*, 4059–4061. [CrossRef]
16. Sixdenier, F.; Yade, O.; Martin, C.; Breard, A.; Vollaire, C. How to include frequency dependent complex permeability into SPICE models to improve EMI filters design? *AIP Adv.* **2018**, *8*, 056604. [CrossRef]
17. Taki, J.; Bensetti, M.; Sadarnac, D. SPICE-compatible high frequency physical modeling approach for an inductor. In Proceedings of the ICPE-ECCE Asia Conference, Seoul, Korea, 1–5 June 2015. [CrossRef]
18. Fiorillo, F.; Kupferling, M.; Appino, C. Magnetic hysteresis and barkausen noise in plastically deformed steel sheets. *Metal* **2018**, *8*, 15. [CrossRef]
19. Xiong, X.; Hu, S.; Hu, K.; Zeng, S. Texture and magnetic property evolution of non-oriented Fe–Si steel due to mechanical cutting. *J. Magn. Magn. Mater.* **2016**, *401*, 982–990. [CrossRef]
20. Deam, A.; Sergeant, P.; Dupre, L.; Chaudhuri, S.; Bliznuk, V.; Kestens, L. Magnetic properties of silicon steel after plastic deformation. *Materials* **2020**, *13*, 4361. [CrossRef]
21. Paltanea, G.; Manescu, V.; Stefanoiu, R.; Nemoianu, I.V.; Gavrila, H. Correlation between magnetic properties and chemical composition of non-oriented electrical steels cut through different technologies. *Materials* **2020**, *13*, 1455. [CrossRef]
22. Sundaria, R.; Lehikoinen, A.; Arkkio, A.; Hannukainen, A. Higher-order finite element modeling of material degradation due to cutting. In Proceedings of the IEMDC, Miami, FL, USA, 21–24 May 2017; pp. 1–7.
23. Vandenbossche, L.; Jacobs, S.; Henrotte, F.; Hameyer, K. Impact of cut edges on magnetization curves and iron losses in e-machines for automotive traction. *World Electr. Veh. J.* **2010**, *4*, 587–596. [CrossRef]
24. Bali, M.; De Gersem, H.; Muetze, A. Finite-element modeling of magnetic material degradation due to punching. *IEEE Trans. Magn.* **2014**, *50*, 7018404. [CrossRef]
25. Weiss, H.A.; Trober, P.; Golle, R.; Volk, W.; Steentjes, S.; Leuning, N.; Elfgen, S.; Hameyer, K. Impact of punching parameter variations on magnetic properties of non-grain oriented electrical steels. *IEEE Trans. Ind. Appl.* **2018**, *54*, 5869–5878. [CrossRef]
26. Sundaria, R.; Lehikoinen, A.; Hannukainen, A.; Arkkio, A.; Belahcen, A. Mixed-order finite-element modeling of magnetic material degradation due to cutting. *IEEE Trans. Magn.* **2018**, *54*, 7402008. [CrossRef]

27. von Pfingsten, G.; Steentjes, S.; Thul, A.; Herold, T.; Hameyer, K. Soft magnetic material degradation due to manufacturing process: A comparison of measurements and numerical simulations. In Proceedings of the ICEMS, Hangzou, China, 22–25 October 2014; pp. 2018–2024.
28. Gmyrek, Z.; Lefik, M.; Cavagnino, A.; Ferraris, L. Comparison of the fractional power motor with cores made of various magnetic materials. *Open Phys.* **2017**, *15*, 827–832. [CrossRef]
29. Gmyrek, Z.; Cavagnino, A. Influence of punching, welding, and clamping on magnetic cores of fractional kilowatt motors. *IEEE Trans. Ind. Appl.* **2018**, *54*, 4123–4132. [CrossRef]
30. Cavagnino, A.; Bojoi, R.; Gmyrek, Z.; Lefik, M. Stator lamination geometry influence on the building factor of synchronous reluctance motor cores. *IEEE Trans. Ind. Appl.* **2017**, *53*, 3394–3403. [CrossRef]
31. Bojoi, R.; Cavagnino, A.; Gmyrek, Z.; Lefik, M. Experimental Assessment of the annealing effects on magnetic core of fractional power synchronous reluctance motors. In Proceedings of the International Conference on Electrical Machines (ICEM), Lausanne, Switzerland, 4–7 September 2016. [CrossRef]
32. Mach, M.; Hajek, V. Model of a small induction machine with effect of manufacturing. In Proceedings of the EDPE Conference, Tatranska Lomnica, Slovakia, 21–23 September 2015. [CrossRef]
33. Bali, M.; De Gersem, H.; Muetze, A. Determination of original nondegraded and fully degraded magnetic characteristics of material subjected to laser cutting. *IEEE Trans. Ind. Appl.* **2017**, *53*, 4242–4251. [CrossRef]
34. de Campos, M.; Yonamine, T.; Fukuhara, M.; Landgraf, F.; Achete, C.; Missell, F. Effect of frequency on the iron losses of 0.5% and 1.5% Si nonoriented electrical steels. *IEEE Trans. Magn.* **2006**, *42*, 2812–2814. [CrossRef]
35. Nemoianu, I.-V.; Manescu, V.; Palnatea, G.; Pascalu, M.-I.; Ciuceanu, R. Electric motors of large consumer products, challenges and trends from the perspective of power efficiency improvement through modern cutting technologies. In Proceedings of the ZINC Conference, Novy Sad, Serbia, 29–30 May 2019; pp. 76–81. [CrossRef]